

Chapter 2

Density-matrix method for coherent accumulation in a multi-level atom

We will now study coherent accumulation in a multi-level atom interacting with a train of ultrashort pulses. For the situation where the atomic relaxation times are longer than the interpulse interval τ , the atomic coherence will survive between two consecutive pulses, leading to *coherent accumulation of excitation* in the sample. Constructive/destructive interference among the coherences excited by the train of pulses will determine the final atomic populations. We will focus on the accumulative effects occurring in the sequential 5S-5P-5D two-photon transitions.

The interaction of the femtosecond comb with the atoms is modeled starting with the Liouville equation for the density matrix of all the atomic states in the laser bandwidth accessible through two-photon absorption, with radiative relaxation included via phenomenological decay terms. The density matrix equations are solved to a fourth-order perturbative expansion in the electric field. With the approximation of impulsive optical excitation during the pulse, followed by free evolution and decay, an iterative numerical procedure is used to determine the state of the atomic system after an arbitrary number of pulses.

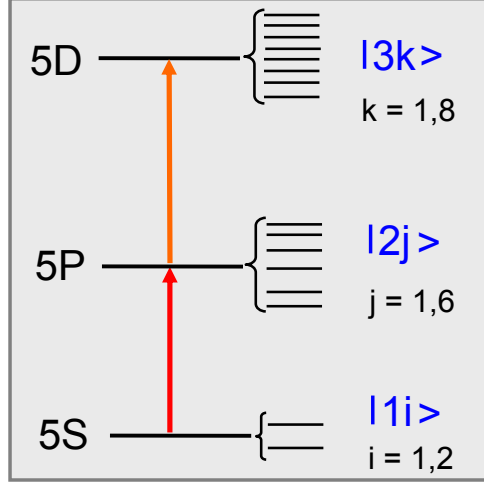


Figure 2.1: Cascade configuration for a multi-level atom.

2.1 Modeling coherent interactions

Consider an electric field $E(t)$ interacting with a multi-level atom in which all the levels are distributed in three different manifolds $|1i\rangle$, $|2j\rangle$ and $|3k\rangle$, in a cascade configuration, as presented in Fig. 2.1. Here ‘1’ labels the ground 5S states, ‘2’ the intermediate 5P states and ‘3’ the excited 5D states, while i , j and k stand for the various fine and hyperfine levels of a specific state. We adopted this simplified notation for the energy levels only in the theory chapter, because it will make the following equations easier to follow.

The Hamiltonian of the system \hat{H} is given by the sum of the field-free atomic Hamiltonian \hat{H}_0 and the interaction potential between the atom and the electric field in the electric-dipole approximation \hat{H}_{int} . Thus, $\hat{H} = \hat{H}_0 + \hat{H}_{int}$, with

$$\begin{aligned} \hat{H}_0 &= \sum_i E_{1i} |1i\rangle\langle 1i| + \sum_j E_{2j} |2j\rangle\langle 2j| + \sum_k E_{3k} |3k\rangle\langle 3k| \quad \text{and} \\ \hat{H}_{int} &= - \sum_{i,j} \mu_{1i,2j} E(t) |1i\rangle\langle 2j| + \sum_{j,k} \mu_{2j,3k} E(t) |2j\rangle\langle 3k| + h.c., \end{aligned} \quad (2.1)$$

where E_{1i} , E_{2j} , E_{3k} are the energies of levels $|1i\rangle$, $|2j\rangle$ and $|3k\rangle$, respectively, and $\mu_{i,j}$ is the dipole moment of the $i \rightarrow j$ transition.

We are interested in the time evolution of the state of the system after a long sequence of pulses. This temporal evolution is described by the Bloch equations, derived from the Liouville equations upon inclusion of the relaxation terms. The starting point is therefore the Liouville equation for the density-matrix elements of the multi-level atomic system, resulting in 9 families of equations for the ground-, intermediate- and excited-state populations, the intra-ground-, intra-intermediate- and intra-excited-state coherences, as well as the 1-2, 2-3 and 1-3 coherences. For clarity, I will write out some representative Liouville equations, for the ground-state populations, ground-state coherences and the 1-2 coherences, respectively:

$$\begin{aligned}
\frac{\partial \rho_{1i,1i}}{\partial t} &= -\frac{i}{\hbar} \langle 1i | [\widehat{H}, \widehat{\rho}] | 1i \rangle \quad \text{ground-state population} \\
\frac{\partial \rho_{1i,1s}}{\partial t} &= -\frac{i}{\hbar} \langle 1i | [\widehat{H}, \widehat{\rho}] | 1s \rangle, \quad \mathbf{s} \neq \mathbf{i} \quad \text{intra-ground-state coherence} \\
\frac{\partial \rho_{1i,2j}}{\partial t} &= -\frac{i}{\hbar} \langle 1i | [\widehat{H}, \widehat{\rho}] | 2j \rangle \quad \text{1-2 coherence.}
\end{aligned} \tag{2.2}$$

The 6 remaining families can be written in a similar manner.

The Bloch equations are obtained from the Liouville equations after including the relaxation rates $\Gamma_{i,j}$ of the (i,j) density matrix components. Note that for our case, $\Gamma_{1i,1i} = 0$, all the population decay rates for a given state are equal, i.e. $\Gamma_{2j,2j} = \Gamma_{5P} \equiv \Gamma_2$ and $\Gamma_{3k,3k} = \Gamma_{5D} \equiv \Gamma_3$, and $\Gamma_{i,j} = \frac{1}{2} (\Gamma_{i,i} + \Gamma_{j,j})$. The subscripts indicating the states in the Γ coefficients will all be kept in the following derivation, for symmetry of the equations. As an example, I will write the Bloch equation for the 1-2 coherence:

$$\frac{\partial \rho_{1i,2j}}{\partial t} = -i\omega_{1i,2j} \rho_{1i,2j} - \frac{i}{\hbar} \langle 1i | [\widehat{H}_{int}, \widehat{\rho}] | 2j \rangle - \Gamma_{1i,2j} \rho_{1i,2j} \tag{2.3}$$

This was obtained by substituting the expression for the Hamiltonian \widehat{H} in Eq. 2.2, with $\omega_{i,j} \equiv (E_i - E_j)/\hbar$. All the coherence equations look the same as Eq. 2.3, with only the appropriate change of indices.

Before writing expressions for the populations of levels $|1\rangle$ and $|2\rangle$, we must also consider the incoherent feeding of level $|2\rangle$ by level $|3\rangle$ and $|1\rangle$ by $|2\rangle$ present in a multi-

level atomic system. Including these additional terms gives the populations as

$$\begin{aligned}
\frac{\partial \rho_{1i,1i}}{\partial t} &= -\frac{i}{\hbar} \langle 1i | [\hat{H}_{int}, \hat{\rho}] | 1i \rangle - \Gamma_{1i,1i} \rho_{1i,1i} + \sum_r \gamma_{1i,r} \rho_{r,r} \\
\frac{\partial \rho_{2j,2j}}{\partial t} &= -\frac{i}{\hbar} \langle 2j | [\hat{H}_{int}, \hat{\rho}] | 2j \rangle - \Gamma_{2j,2j} \rho_{2j,2j} + \sum_r \gamma_{2j,r} \rho_{r,r} \\
\frac{\partial \rho_{3k,3k}}{\partial t} &= -\frac{i}{\hbar} \langle 3k | [\hat{H}_{int}, \hat{\rho}] | 3k \rangle - \Gamma_{3k,3k} \rho_{3k,3k}.
\end{aligned} \tag{2.4}$$

More details about deriving the incoherent feeding terms will be given in 2.1.2.

We can now integrate Eqs. 2.3 and 2.4, with the assumption of *impulsive optical excitation* during the interaction time: the pulse duration is ultrashort compared to the pulse repetition period or any relaxation time of the system, as seen from Table 2.1.

Pulse duration	~ 30 fs
Laser repetition period	10 ns
5P lifetime	27 ns [36]
5D lifetime	240 ns [36]
1-2 coherence lifetime	54 ns
1-3 coherence lifetime	480 ns
2-3 coherence lifetime	48.5 ns

Table 2.1: Relevant times for the interaction of the femtosecond laser with the ^{87}Rb atoms.

This means that the interaction potential \hat{H}_{int} changes on a very fast timescale compared to the $\Gamma_{i,j}$ relaxation rates, allowing us to neglect the temporal dependence on $\Gamma_{i,j}$ inside the integrals containing \hat{H}_{int} , and yielding:

$$\begin{aligned}
\rho_{1i,1i}(t) &= e^{-\Gamma_{1i,1i} t} \left[\rho_{1i,1i}^0 - \frac{i}{\hbar} \int_0^t dt' \langle 1i | [\hat{H}_{int}, \hat{\rho}] | 1i \rangle + \sum_r \gamma_{1i,r} \int_0^t dt' e^{\Gamma_{1i,1i} t'} \rho_{r,r}(t') \right] \\
\rho_{1i,2j}(t) &= e^{-i\omega_{1i,2j} t - \Gamma_{1i,2j} t} \left[\rho_{1i,2j}^0 - \frac{i}{\hbar} \int_0^t dt' e^{i\omega_{1i,2j} t'} \langle 1i | [\hat{H}_{int}, \hat{\rho}] | 2j \rangle \right]
\end{aligned} \tag{2.5}$$

for the ground-state population and 1-2 coherence, respectively.

Numerical integration of Eq. 2.5 gives the time evolution of the system with arbitrary initial conditions, but is computationally challenging for the ^{87}Rb atom, where there are *two* 5S initial levels, *six* 5P intermediate levels and *eight* 5D final levels,

leading to a total of $16^2 = 256$ coupled Bloch equations. To avoid the long computational times, our collaborator Daniel Felinto [37,38] has developed an iterative numerical procedure that determines the state of the atomic system after any number of pulses. As previously mentioned, for laser repetition periods τ shorter than the relaxation times of the system, as is the case of ^{87}Rb , the atomic sample will accumulate excitation in the form of population and coherence.

In Daniel Felinto's iterative solution, the state of the system before the $(n + 1)$ -th pulse in the train is obtained from the state prior to the n -th pulse. The relation connecting ρ^{n+1} to ρ^n is easily derived from Eq. 2.5 by setting $t = \tau$. Again, making the *impulsive optical excitation* assumption means setting $t \rightarrow \infty$ in all the integrals containing \hat{H}_{int} ; the lower limit can be made $t \rightarrow -\infty$, since $E(t) = 0$ for $t < 0$. For the two sample elements of the density matrix appearing in Eq. 2.5 we obtain

$$\begin{aligned}\rho_{1i,1i}^{n+1} &= e^{-\Gamma_{1i,1i}\tau} \left[\rho_{1i,1i}^c + \sum_r \gamma_{1i,r} \int_0^\tau dt' e^{\Gamma_{1i,1i}t'} \rho_{r,r}(t') \right] \\ \rho_{1i,2j}^{n+1} &= e^{-i\omega_{1i,2j}\tau - \Gamma_{1i,2j}\tau} \left[\rho_{1i,2j}^c \right],\end{aligned}\quad (2.6)$$

where

$$\rho_{r,s}^c = \rho_{r,s}^n - \frac{i}{\hbar} \int_{-\infty}^{\infty} dt' e^{i\omega_{r,s}t'} \langle r | [\hat{H}_{int}^n, \hat{\rho}] | s \rangle \quad (2.7)$$

is the density matrix coherently excited by the n -th pulse (\hat{H}_{int}^n), a function of the initial state prior to the n -th pulse ρ^n . Expressions similar to Eq. 2.6 are derived for the 7 remaining families of equations.

As a demonstration, Fig. 2.2 (adapted from Felinto *et al.*, reference [38]) shows the temporal evolution of the ρ_{22} and ρ_{33} populations in a *three-level* atom interacting with a train of hyperbolic-secant pulses. The total number of coupled Bloch equations for this system is $3^2 = 9$, so a direct numerical integration is not yet computationally intensive. The solid lines are a result of the direct numerical integration (~ 1.5 hours of computational time), while the open circles arise from successive applications of Eq. 2.6 to the atom initially in the ground state (< 10 s). The transient behavior of the excited

level populations is governed by their significantly different (factor of 10) lifetimes, as demonstrated by the different timescales in the two frames of the figure.

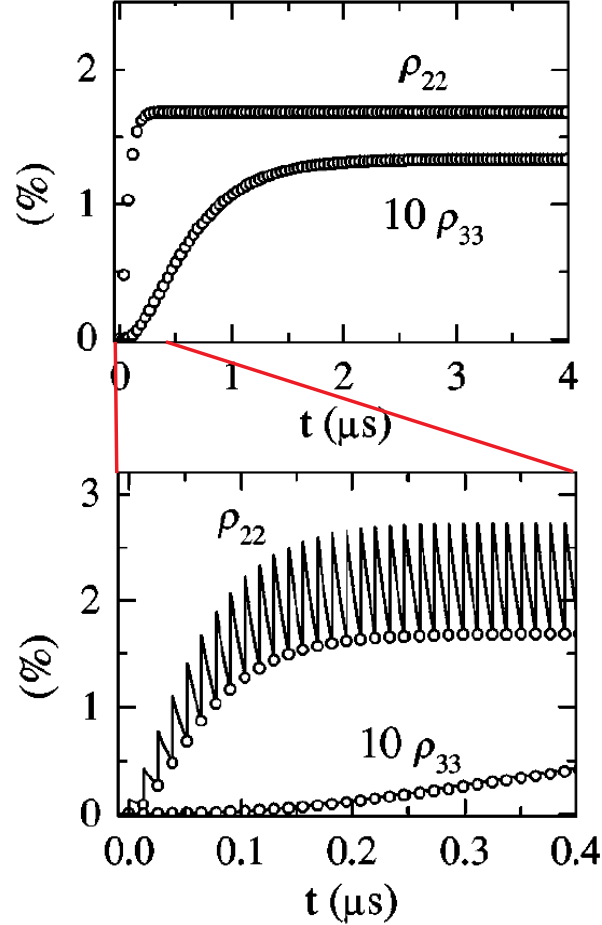


Figure 2.2: (adapted from reference [38]) Time evolution of the populations ρ_{22} and ρ_{33} for a *three-level* atom interacting with a train of hyperbolic-secant pulses. The two frames are different timescales of the same evolution, where the solid lines are a result of direct numerical integration of the Bloch equations and the open circles come from successive applications of Eq. 2.6.

After a large number of pulses, the system reaches a stationary state that repeats every τ . The shape of the direct-integration curve accounts for the very fast change in population during the pulse interaction time, followed by a slow decay in between pulses. The numerical-iteration method agrees well with the direct integration, in that it always matches the value at the minimum. This happens because, in the iteration

procedure, the initial state is always taken to be the state ρ^n just before the impulsive excitation. The situation would be reversed and the two curves would match at the maximum if the initial state were the state immediately after each individual pulse.

To summarize, in the simplified treatment of coherent accumulation for a two-photon process in a multi-level atom, there are two major steps: the first is obtaining the state of the system after the interaction with a pulse in the train, for an arbitrary initial state of the atom (Eq. 2.6). The second step is the successive application of Eq. 2.6, yielding the atomic state after a sequence of pulses, or in other words, describing the time evolution of the system.

2.1.1 The coherently excited density matrix ρ^c

There are two quantities left to calculate now, the coherently excited density matrix in Eq. 2.7, associated with the impulsive excitation during the laser pulse, and the feeding terms in Eq. 2.4, arising from incoherent decay.

We will first focus on ρ^c , realizing that it is a product of two probability amplitudes in the interaction picture

$$\rho_{i,j}^c = C_i \times C_j^*, \quad C_i = \langle i | \hat{U}_I(t) | \Psi_0 \rangle, \quad (2.8)$$

with Ψ_0 the initial state of the system, which is a superposition of all the atomic states, and $\hat{U}_I(t)$ the time propagation operator in the interaction picture, given by

$$\hat{U}_I(t) = 1 + \left(-\frac{i}{\hbar}\right) \int_0^t dt' \hat{H}_{int}^I(t') + \left(-\frac{i}{\hbar}\right)^2 \int_0^t dt' \int_0^{t'} dt'' \hat{H}_{int}^I(t') \hat{H}_{int}^I(t'') + \dots \quad (2.9)$$

After inserting the relation for $\hat{H}_{int}^I(t)$, $\hat{H}_{int}^I(t) = e^{i\hat{H}_0 t/\hbar} \hat{H}_{int}(t) e^{-i\hat{H}_0 t/\hbar}$, and specifying the electric field $E(t) = \mathcal{E}(t)e^{i\omega t + i\phi_0} + c.c.$ as defined in section 1.3, we obtain the following general expressions for the three groups of probability amplitudes:

$$C_{3k}(t) = \sum_s A_{3k,3s} C_{3s}^0 + \sum_j A_{3k,2j} e^{-i\phi_0} C_{2j}^0 + \sum_i A_{3k,1i} e^{-2i\phi_0} C_{1i}^0 \quad (2.10)$$

$$\begin{aligned}
C_{2j}(t) &= \sum_k A_{2j,3k} e^{i\phi_0} C_{3k}^0 + \sum_s A_{2k,2s} C_{2s}^0 + \sum_i A_{2j,1i} e^{-i\phi_0} C_{1i}^0 \\
C_{1i}(t) &= \sum_k A_{1i,3k} e^{2i\phi_0} C_{3k}^0 + \sum_j A_{1i,2j} e^{i\phi_0} C_{2j}^0 + \sum_s A_{1i,1s} C_{1s}^0,
\end{aligned}$$

where $A_{i,j}$ are the Dyson coefficients corresponding to the time evolution from state i to state j . This yields the final formula for any element (i, j) of the impulsively excited density matrix ρ^c

$$\rho_{i,j}^c = e^{-iB_{i,j}\phi_0} \sum_{r,s} A_{i,r} A_{j,s}^* e^{iB_{r,s}\phi_0} \rho_{r,s}^0, \quad (2.11)$$

with $B_{i,j} = 2\sum_k(\delta_{3k,i} - \delta_{3k,j}) + \sum_k(\delta_{2k,i} - \delta_{2k,j})$, where the δ s are Kronecker symbols.

We are interested in developing a theory in *the weak-field regime*: from the infinite Dyson series only the terms up to the fourth order in the electric field will be kept. The fourth order is the smallest order contributing to population in the most excited level for two-photon transitions from the ground state. In this regime, making *the rotating-wave approximation* will result in expressions for the 9 groups of elements $A_{i,j}$ present in Eqs. 2.10 and 2.11. As an example, I will write out the expression for $A_{3k,3s}$:

$$\begin{aligned}
A_{3k,3s} &= \delta_{3k,3s} + \left(-\frac{iea_0}{\hbar}\right)^2 \sum_r m_{3k,2r} m_{2r,3s} \int_0^t dt' \int_0^{t'} dt'' e^{i\delta_{3k,2r}t'} e^{i\delta_{2r,3s}t''} \mathcal{E}^*(t') \mathcal{E}(t'') \\
&+ \left(-\frac{iea_0}{\hbar}\right)^4 \sum_{r,n,q} m_{3k,2r} m_{2r,1n} m_{1n,2q} m_{2q,3s} \int_0^t dt' \int_0^{t'} dt'' \int_0^{t''} dt''' \int_0^{t'''} dt'''' e^{i\delta_{3k,2r}t'} \\
&\times e^{i\delta_{2r,1n}t''} e^{i\delta_{1n,2q}t'''} e^{i\delta_{2q,3s}t''''} \mathcal{E}^*(t') \mathcal{E}^*(t'') \mathcal{E}(t''') \mathcal{E}(t''') + \left(-\frac{iea_0}{\hbar}\right)^4 \\
&\times \sum_{r,n,q} m_{3k,2r} m_{2r,3n} m_{3n,2q} m_{2q,3s} \int_0^t dt' \int_0^{t'} dt'' \int_0^{t''} dt''' \int_0^{t'''} dt'''' e^{i\delta_{3k,2r}t'} e^{i\delta_{2r,3n}t''} \\
&\times e^{i\delta_{3n,2q}t'''} e^{i\delta_{2q,3s}t''''} \mathcal{E}^*(t') \mathcal{E}(t'') \mathcal{E}^*(t''') \mathcal{E}(t'''), \quad (2.12)
\end{aligned}$$

with $\delta_{i,j} \equiv \omega_{i,j} - \omega_c$ the detunings relative to the carrier frequency, $m_{i,j} = \mu_{i,j}/ea$ dimensionless dipole moments, e the electron charge and a the Bohr radius. The last three terms in Eq. 2.12 are second-order and fourth-order contributions to the excitation, related to the processes of absorption and stimulated emission on the lower and upper transitions. They are schematically drawn in Fig. 2.3.

This messy expression can be greatly simplified if we consider the situation where

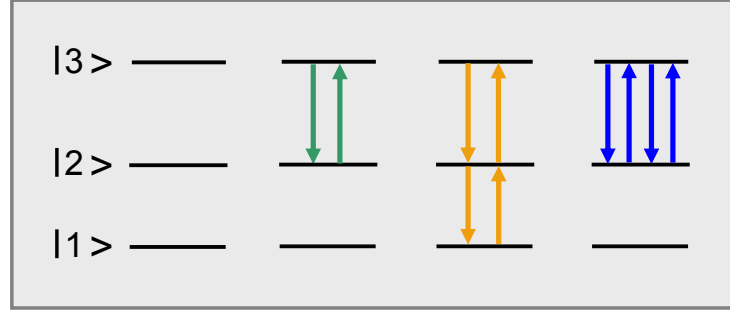


Figure 2.3: Vector diagrams for the four terms present in Eqs. 2.12 and 2.13 for the sample Dyson coefficient.

the pulse is ultrashort compared to the time variation determined by the atomic detunings, i.e. we neglect all the exponentials in Eq. 2.12, and if we limit ourselves to the reasonable case of a *real envelope function*. Under these approximations, the nested integrals take a much simpler form, via successive integration by parts, with the result

$$\begin{aligned}
 A_{3k,3s} &= \delta_{3k,3s} - \frac{\theta^2}{2!} \sum_r m_{3k,2r} m_{2r,3s} + \\
 &+ \frac{\theta^4}{4!} \left(\sum_{r,n,q} m_{3k,2r} m_{2r,1n} m_{1n,2q} m_{2q,3s} + \sum_{r,n,q} m_{3k,2r} m_{2r,3n} m_{3n,2q} m_{2q,3s} \right).
 \end{aligned} \tag{2.13}$$

Here θ is the pulse area, defined as

$$\theta = \frac{ea}{\hbar} \int_{-\infty}^{\infty} dt \mathcal{E}(t) \quad \text{pulse area.} \tag{2.14}$$

2.1.2 The incoherent feeding terms

There are two very different timescales over which the populations present in the feeding-term integrals vary: first, there is a very fast change in population during the pulse interaction time, followed by a slow, incoherent decay during the interpulse interval. In this model, it is assumed for simplicity that level $|2\rangle$ is fed only by level $|3\rangle$, and $|1\rangle$ is only fed by $|2\rangle$. Note that the population in the latter level varies in time due to feeding from $|3\rangle$. However, in reality, there are two decay channels for the 5D population [36], as illustrated in Fig. 2.4: the first is the 5D-5P-5S radiative cascade

and the second is the 5D-6P-5S cascade. In fact, we experimentally determine the 5D population by detecting the 420 nm blue fluorescence emitted in the 6P-5S transition. The 6P state is not included in the simulation.

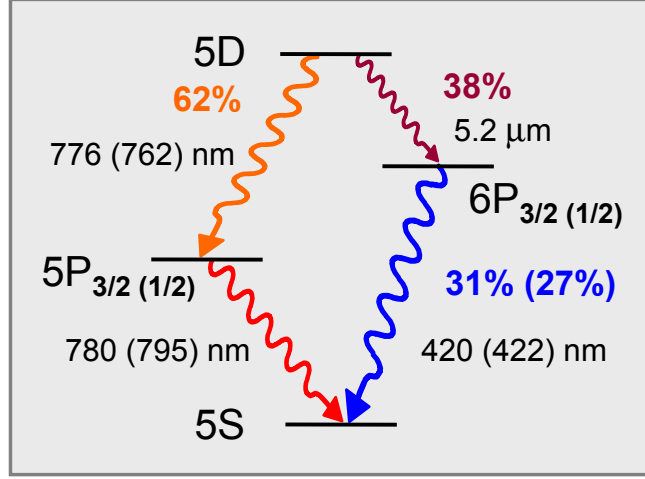


Figure 2.4: Decay paths for the 5D levels of ^{87}Rb , with the corresponding transition wavelengths and branching ratios specified. In the experiment, we detect the 6P-5S blue photons at 420 nm, which represent roughly 10% of the 5D population. The 6P levels also decay to the 6S and 4D levels, not pictured here.

For the situation where the pulse duration is ultrashort compared to the laser repetition period τ and considering only the 5P decay channel for the 5D population, we have:

$$\begin{aligned} \sum_k \gamma_{2j,3k} \int_0^\tau dt' e^{\Gamma_{2j,2j} t'} \rho_{3k,3k}(t') &\simeq \sum_k \gamma_{2j,3k} \rho_{3k,3k}^c \int_0^\tau dt' e^{\Gamma_{2j,2j} t'} e^{-\Gamma_{3k,3k} t'} \\ &= \sum_k \gamma_{2j,3k} \rho_{3k,3k}^c \frac{1 - e^{(\Gamma_{2j,2j} - \Gamma_{3k,3k})\tau}}{\Gamma_{3k,3k} - \Gamma_{2j,2j}} \end{aligned} \quad (2.15)$$

$$\begin{aligned} \sum_j \gamma_{1i,2j} \int_0^\tau dt' e^{\Gamma_{1i,1i} t'} \rho_{2j,2j}(t') &\simeq \sum_j \gamma_{1i,2j} \int_0^\tau dt' e^{\Gamma_{1i,1i} t'} e^{-\Gamma_{2j,2j} t'} \\ &\times \left[\rho_{2j,2j}^c + \sum_k \gamma_{2j,3k} \int_0^{t'} dt'' e^{\Gamma_{2j,2j} t''} \rho_{3k,3k}(t'') \right] \\ &= \sum_j \gamma_{1i,2j} \rho_{2j,2j}^c \frac{1 - e^{(\Gamma_{1i,1i} - \Gamma_{2j,2j})\tau}}{\Gamma_{2j,2j} - \Gamma_{1i,1i}} + \sum_j \sum_k \frac{\gamma_{1i,2j} \gamma_{2j,3k}}{\Gamma_{2j,2j} - \Gamma_{3k,3k}} \end{aligned}$$

$$\times \rho_{3k,3k}^c \left[\frac{1 - e^{(\Gamma_{1i,1i} - \Gamma_{3k,3k})\tau}}{\Gamma_{3k,3k} - \Gamma_{1i,1i}} - \frac{1 - e^{(\Gamma_{1i,1i} - \Gamma_{2j,2j})\tau}}{\Gamma_{2j,2j} - \Gamma_{1i,1i}} \right]. \quad (2.16)$$

After realizing that $\Gamma_{1i,1i} = 0$ and that all the population decay rates for a given state are equal, i.e. $\Gamma_{2j,2j} = \Gamma_2$, $\Gamma_{3k,3k} = \Gamma_3$, after setting the feeding coefficients proportional to the branching ratios of the upper levels down to the lower levels $\gamma_{2j,3k} = r_{2j,3k}\Gamma_3$, $\gamma_{1i,2j} = r_{1i,2j}\Gamma_2$ and defining the following constants $D_{32} = \Gamma_3 \frac{1 - \exp(\Gamma_2 - \Gamma_3)\tau}{\Gamma_3 - \Gamma_2}$, $D_{21} = 1 - \exp(-\Gamma_2\tau)$ and $D_{321} = \frac{\Gamma_2\Gamma_3}{\Gamma_2 - \Gamma_3} \left[\frac{1 - \exp(-\Gamma_3\tau)}{\Gamma_3} - \frac{1 - \exp(-\Gamma_2\tau)}{\Gamma_2} \right]$, the final expression for the populations after the n -th pulse becomes:

$$\begin{aligned} \rho_{1i,1i}^{n+1} &= \rho_{1i,1i}^c + D_{21} \sum_j r_{1i,2j} \rho_{2j,2j}^c + D_{321} \sum_j r_{1i,2j} \sum_k r_{2j,3k} \rho_{3k,3k}^c \\ \rho_{2j,2j}^{n+1} &= e^{-\Gamma_2\tau} \left[\rho_{2j,2j}^c + D_{32} \sum_k r_{2j,3k} \rho_{3k,3k}^c \right] \\ \rho_{3k,3k}^{n+1} &= e^{-\Gamma_3\tau} \rho_{3k,3k}^c, \end{aligned} \quad (2.17)$$

where $\rho_{i,j}^c$ are given by Eq. 2.11.

2.2 Summary of the coherent interaction model

The relevant laser parameters for describing the interaction of the femtosecond comb with the atoms are the interpulse period τ , the carrier envelope phase evolution between successive pulses $\delta\phi$, the pulse duration and its associated area θ . The model includes the fine and hyperfine structure of the 5S, 5P and 5D states, with energy-level information provided by the literature. The Zeeman substructure is averaged over, for linear polarization. In the simulation, calculated oscillator strengths and Clebsch-Gordan coefficients are employed for all the involved transition pathways in an effort to accurately predict the relative signal strengths. This general set of coupled Bloch-type equations, evolving from one pulse to the next, leads to a global picture of coherent population accumulation and incoherent optical pumping.

For times that are short compared to the atomic decoherence time, the femtosecond pulse train drives the atomic coherence in phase such that a multi-pulse excitation

is coherently built up for resonant atomic states. At longer times, however, the coherence in the optical field can no longer be transferred to the atom owing to the finite atomic coherence time. Incoherent processes such as optical pumping then govern the population transfer dynamics.

These two timescales of the system, excitation and optical pumping, can be clearly seen in Fig. 2.5 (a) which shows the time evolution for two different two-photon resonances. The two curves have the same coherent excitation timescale of a few microseconds, set by the 5S-5D coherence lifetime of ~ 500 ns. The slow decay rate is different though for each transition. Figure 2.5 (b) illustrates the behavior of one of the transitions as a function of the detuning from resonance. On resonance, all the pulses in the train contribute to the excitation, since the train of pulses is in phase with the atomic frequency. Away from resonance, the decrease in population due to destructive interference is accompanied by oscillations in the excitation region, arising from the phase difference between the atomic frequency and the frequency of the closest comb line. This oscillatory behavior at the frequency difference is more obvious in Fig. 2.5 (c), where the detuning from resonance is even larger.

2.3 Coherent accumulation enables high resolution

Temporal coherent control is best manifested in the 5D coherent population accumulation and transition linewidth evolution, which reach their asymptotic limits imposed by the atomic decoherence, through the coherent interaction with the train of femtosecond pulses. The results of the model (Fig. 2.6), under the condition of a small pulse area, illustrate the effect of pulse accumulation on signal strength and spectral linewidth.

The upper graph [(Fig. 2.6 (a))] shows that the on-resonance 5D population increases as the square of the number of pulses until reaching approximately the decoherence time, ~ 500 ns for the 5D states. This 5D signal scaling at short times is reinforced

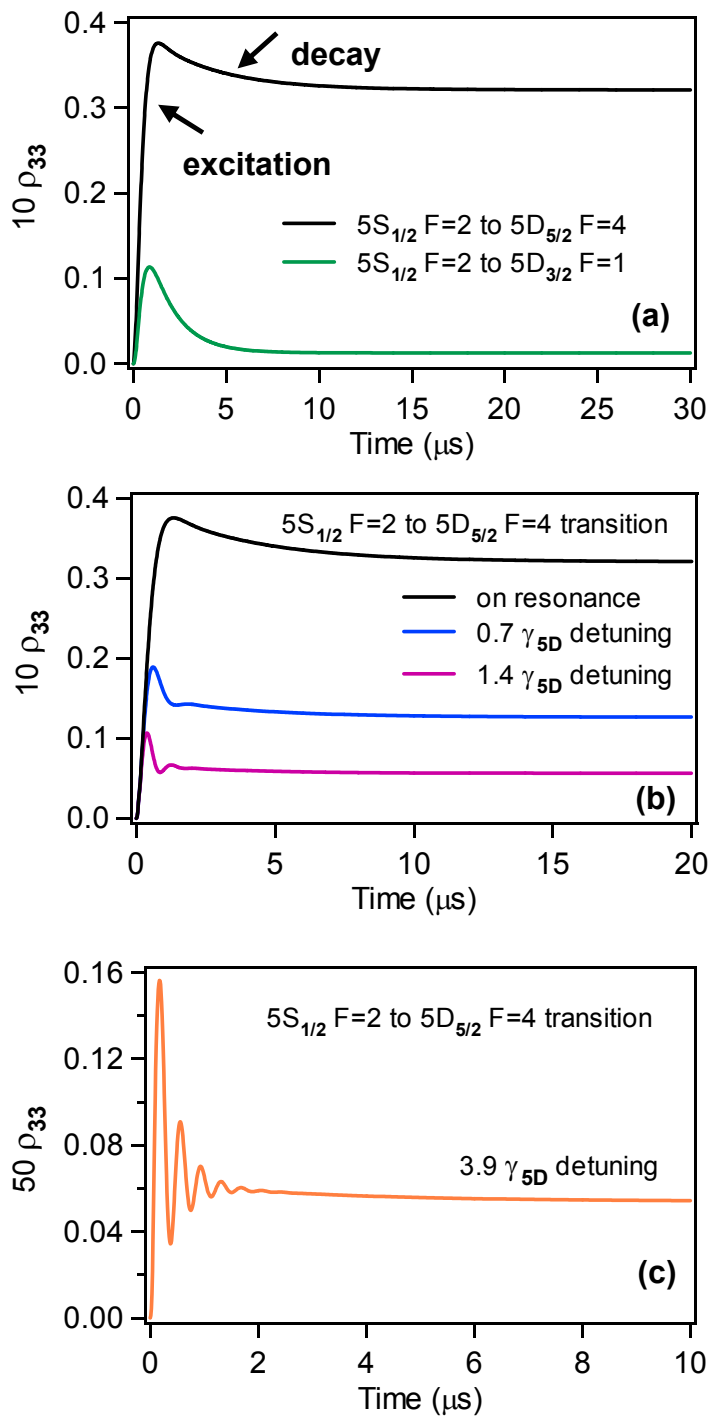


Figure 2.5: Several aspects of population dynamics at short and long timescales: (a) Time evolution for two resonances, showing the short coherent excitation, followed by the slow incoherent decay. (b) Temporal evolution for one of the previous transitions, for different detunings from the atomic resonance, illustrating the destructive interference that results in the out-of-resonance condition. (c) Oscillation resulting from the phase difference between the atomic frequency and the train of pulses.

in the figure by a quadratic fit. The proportionality of the transition probability to the squared number of pulses N^2 is a more general result, valid in the weak excitation regime, which was theoretically demonstrated for a two-level atom [39], in agreement with earlier conclusions based on perturbation theory [40].

The rapid population increase is accompanied by the narrowing of the resolution linewidth [(Fig. 2.6 (b)), with the obtained resolution limited only by the 5D natural linewidth. After the very first pulse, the linewidth is the single-pulse bandwidth of the laser; as the pulses keep coming, the spectral components from successive pulses interfere among themselves, resulting in the linewidth decrease. Thus, the atoms are the spectrometer used to observe the frequency comb, and the atomic linewidth is the bandwidth limit of this spectrometer.

The dependence of the 5D population and linewidth versus the number of pulses is temporally analogous to the power density scaling and the spatial resolution versus the number of slits in a multi-slit experiment [39, 40]. Again, this is a general result, valid for a broad range of pulse shapes, pulse areas or detunings. The two effects of coherent pulse accumulation on signal strength and spectral linewidth have both been experimentally verified [41]. The quadratic increase of the excited state population versus the accumulated number of pulses can be further enhanced with a larger f_r , where the shorter pulse interval allows for more pulses to be ‘added’ during the atomic coherence lifetime.

The theoretical model we have developed is designed to predict the coherent accumulation of population in the 5D states, followed by incoherent optical pumping. Using this model we generate atomic transition spectra by tuning either f_r or f_0 . We then compare them with the corresponding experimental spectra (covering the same f_r and f_0 range), as presented in Chapter 5. In addition to comparing theory and experiment, we also use the model prediction to adjust the experimental data. For the

case of the indirect 5P frequency measurements via the 5S-5D two-photon transitions, described in Chapter 6, we use the theoretical prediction to modify the raw data (after the adjustment, the data fall on top of a Lorentzian).

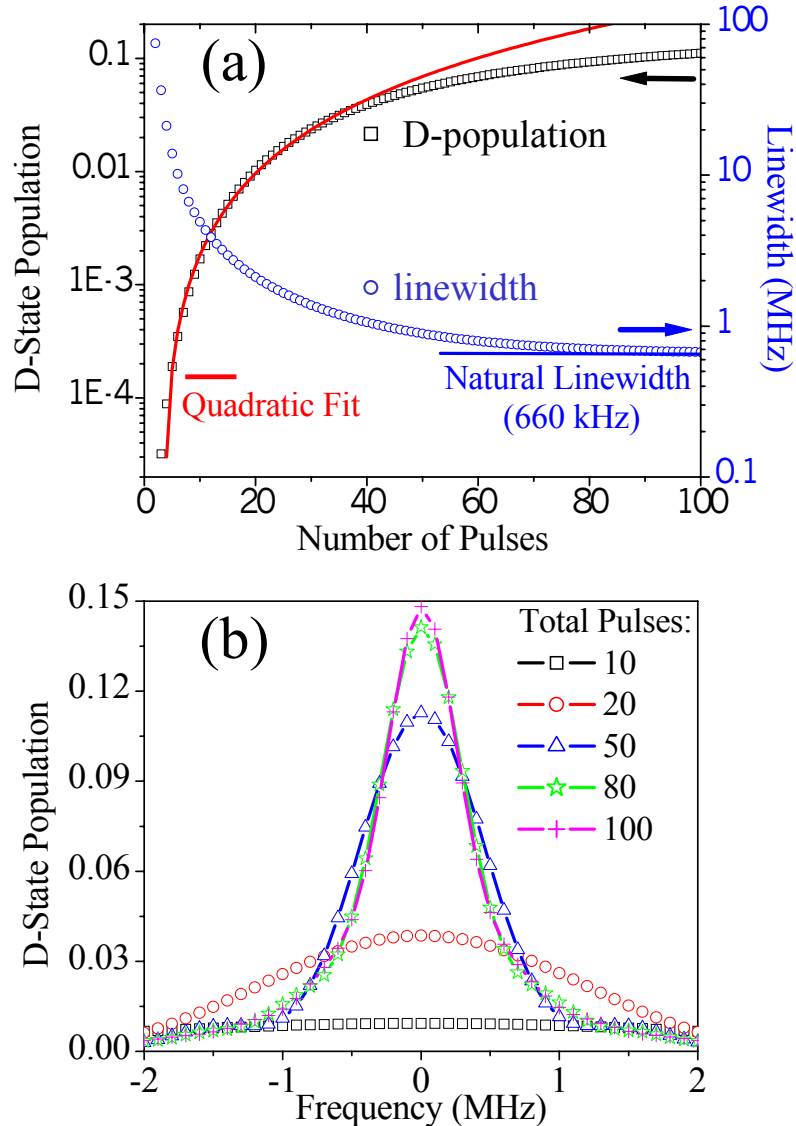


Figure 2.6: (a) Left (right) axis shows calculated 5D population (linewidth) on resonance for the closed two-photon transition versus total number of accumulated pulses. The time between pulses is ~ 10 ns, and the system reaches its asymptotic values of signal amplitude and linewidth after ~ 480 ns. The quadratic fit to the 5D population at short times shows that the signal scales as the square of the number of pulses until atomic decoherence limits the coherent pulse accumulation. (b) The corresponding 5D resonance lineshape versus the number of pulses. During the first 10 pulses, the comb structure is not sufficiently developed to offer appreciable signal or resolution.